Available online at www.sciencedirect.com
ScienceDirect
Journal of the European Ceramic Society 28 (2008) 425–429
www.elsevier.com/locate/jeurceramsoc

Water vapor corrosion of mullite: Single crystals versus polycrystalline ceramics

Martin Schmücker [a,*], Peter Mechnich [a], Stefan Zaefferer [b], Hartmut Schneider [a]

[a] German Aerospace Center, Institute of Materials Research, 51147 Köln, Germany
[b] Max-Planck Institute for Iron Research, 40237 Düsseldorf, Germany

Available online 6 April 2007

Abstract

Water vapor corrosion of mullite single crystals and polycrystalline mullite ceramics was investigated in rapidly streaming water vapor at 1200 °C. Both materials behave quite differently: mullite ceramics display non-isotropic corrosive attack resulting in superficial α-alumina formation with high nucleation density. Preferential corrosion occurs on crystal surfaces oriented more or less perpendicular to the crystallographic *c*-axis (i.e. on or near to the (0 0 1) plane), while parallel to *c* no corrosion effects are observed after short-term treatments. In single crystals, on the other hand, the α-alumina formation rate does not depend on crystal orientation; moreover, the nucleation density of alumina is relatively low. In case of stoichiometric mullite ceramics, having approximately stoichiometric 3/2-mullite composition (i.e. ≈72 wt.% Al_2O_3) the early stage of water vapor-induced mullite to α-alumina conversion is interpreted in terms of true corrosion. This process is stronger parallel to the *c*-axis than perpendicular to it, reflecting the non-isotropic bonding character of mullite. In the case of mullite single crystals, having approximately 2/1-composition (i.e. ≈78 wt.% Al_2O_3) the early stage of mullite/alumina conversion is considered as a hydrothermally activated isotropic α-alumina precipitation process of mullite, supersaturated in Al_2O_3.

Keywords: Mullite; Electron microscopy; Corrosion; Hot water vapor

1. Introduction

Mullite is an excellent material for many high temperature applications. This is due to its high creep resistance, good thermal shock behavior and inherent oxidation stability.[1] However, as many other silicate ceramics, mullite is prone to water vapor hot-corrosion and this may limit the use of mullite ceramics if exposed to combustion environments.

The decomposition of mullite in hot water vapor follows the overall reaction:

$$3Al_2O_3{\cdot}2SiO_2 + 4H_2O \Rightarrow 3Al_2O_3 + 2Si(OH)_4\uparrow \quad (1)$$

As a consequence, if mullite is exposed to water vapor at sufficiently high temperatures, a porous α-alumina layer forms on the ceramic surface.[2,3]

Only little information exists on early stages of mullite corrosion and related mullite-alumina transformation. Rüscher et al.[4] found that H_2O corrosion first causes hydroxylation of the mullite structure. Iwai et al.[5] studied the mullite/alumina conversion using a propane-oxygen gas burner. By means of X-ray diffractometry the topotaxial relation between mullite and α-alumina of $(3\,1\,0)_{Mullite} \| (0\,0\,1)_{\alpha\text{-}Al_2O_3}$ and $[0\,0\,1]_{Mullite} \| [1\,-1\,0]_{\alpha\text{-}Al_2O_3}$ was identified. Orientation relationships between mullite and alumina are currently re-examined by Hildmann and Braue using samples annealed in dry air and argon at temperatures up to 1400 °C.[6] Ueno et al. have investigated hot-pressed mullite ceramics in water vapor under static conditions at 1300 and 1500 °C. It was found that alumina occurring on mullite surfaces was grown from a silica rich sodium-containing aluminosilicate phase.[2] A similar observation was found by Eils et al. after treating mullite single crystal sections in H_2O/O_2 gas mixtures at 1670 °C under relatively slow flowing conditions (100 ml/min).[7] Most recently, we have investigated the conversion of mullite single crystal sections in water vapor of relatively high flow rates (10 m/s) at rather moderate temperature (1200 °C).[8]

In the present contribution, the early stages of water vapor-induced mullite-α-alumina conversion are studied in more detail. The investigations are focused on possible non-isotropic effects of the corrosive attack and on the orientation relationship

* Corresponding author. Tel.: +49 22 03 601 2462; fax: +49 22 03 696 480.
E-mail address: martin.schmuecker@dlr.de (M. Schmücker).

0955-2219/$ – see front matter © 2007 Elsevier Ltd. All rights reserved.
doi:10.1016/j.jeurceramsoc.2007.03.013

Table 1
Chemical composition of mullite $Al_{4+2x}Si_{2-2x}O_{10-x}$

Designation	x	Al_2O_3 (mol %)	SiO_2 (mol %)
Mullite single crystal (fused mullite)	0.40	66	34
Mullite ceramics (sintered mullite)	0.25	60	40

between mullite and α-alumina. Of special interest is the comparison between mullite single crystals and polycrystalline mullite ceramics.

2. Experimental procedure

2.1. Mullite samples

The mullite single crystal used for this study was prepared by Dr. F. Walraffen (University of Bonn, Germany) using Czochralski technique according to Ref.[9]. Crystal slices were cut parallel to (0 0 1) and (0 1 0) mullite planes. Polycrystalline mullite ceramics was prepared by firing pellets of a commercial mullite precursor (Siral28, SASOL, Hamburg, Germany) at 1700 °C. Sample compositions are summarized in Table 1. The sample surfaces were polished with 3 μm diamond spray and subsequently with colloidal silica. Finally, the slices were ion-beam polished using a low angle (15 ° from parallel) between the ion beam and the sample surface.

2.2. Water vapor corrosion tests

The water vapor treatment was performed in a newly installed rig at DLR. The experimental setup consists of an industrial steam generator and a vertical tube furnace. The continuously operating steam source is able to generate water vapor with a mass flow between 1 and 4 kg/h; in the present study the mass flow was 3 kg/h. The steam generator is linked to the tube furnace by a heated hose operating at 175 °C to prevent steam condensation between generator outlet and tube furnace inlet. The samples were heated under flowing steam from 300 to 1200 °C with a heating rate of 10 °/min. After dwell times of 1.5 or 3 h, respectively, samples were cooled with a rate of 20–300 °C. The inner tube cross-section is approximately 6 cm^2, at a mass-flow of 3 kg/h one can estimate a steam velocity of ≈10 m/s at 1200 °C.

2.3. Scanning electron microscopy (SEM) and electron back-scatter diffraction (EBSD)

The determination of crystal orientations was performed by means of electron backscatter diffraction (EBSD) technique. For that, a JEOL 6500 F SEM equipped with an EBSD system (TSL/EDAX with Digiview camera) was employed. A crucial point in EBSD-experiments of non-conductive materials is the application of a suitable coating, thin enough not to absorb the diffracted electrons, yet thick enough to prevent charging effects. In preliminary experiments, a carbon coating of 1 nm thickness applied by ion beam sputtering (GATAN HR ion beam coater) was found to be viable. The EBSD measurements were performed without re-polish of the surface. As a consequence, orientation determination was only possible on those facets of the newly grown crystals that were by chance correctly oriented for the recording of patterns (with a surface normal not deviating more than approximately ±15° from that of the flat single crystal surface).

For pattern indexing the following crystal parameters were used: sillimanite (as simplified representative of mullite): orthorhombic (mmm), $a = 7.486$ Å, $b = 7.675$ Å, $c = 5.773$ Å, α-alumina: trigonal (−3 m), $a = 4.758$ Å, $c = 12.991$ Å

3. Results

3.1. H_2O vapor-treated mullite single crystals

After water vapor treatment at 1200 °C for 1.5 or 3 h relatively large (up to 50 μm) facetted α-alumina crystals have formed on the (0 0 1) and (0 1 0) mullite surfaces (Figs. 1A and 2A). Typically the newly formed alumina crystals occur in clusters with unaffected mullite areas in between. The irregular alumina distribution suggests that structural defects on the surface of the mullite single crystal plates may facilitate the mullite-alumina conversion. Corundum crystals formed on $(0\,0\,1)_{Mullite}$ virtually appear equiaxed; in contrast, on $(0\,1\,0)_{Mullite}$ section small equiaxed crystals and large elongated α-alumina crystals

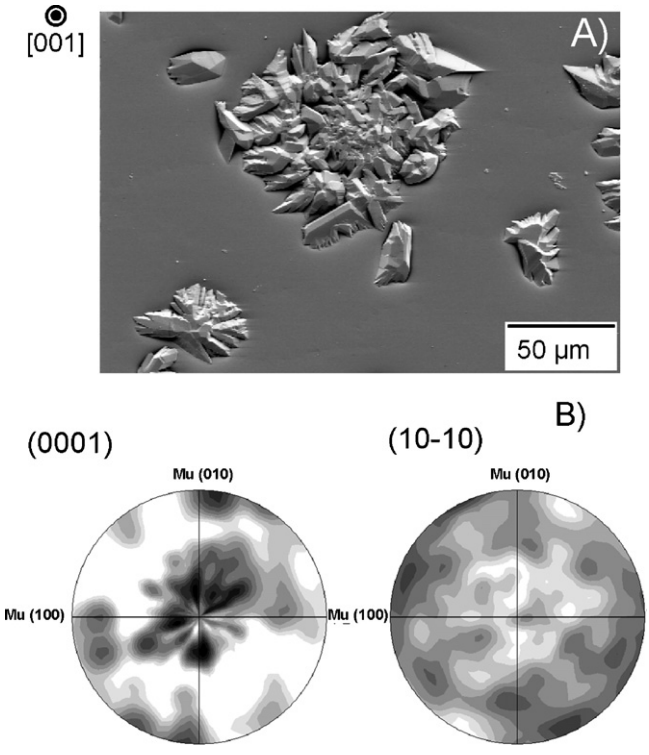

Fig. 1. Alumina formation on water vapor-treated (1200 °C, 3 h) mullite single crystal sections cut parallel to (0 0 1). (A) Microstructure; (B) pole figures of basal (0 0 0 1) and prismatic (1 0 –1 0) planes of α-Al_2O_3. α-Alumina crystals are predominantly oriented according to [0 0 0 1]Cor || [0 0 1]Mul, whereas prismatic corundum crystal planes display a virtually random distribution.

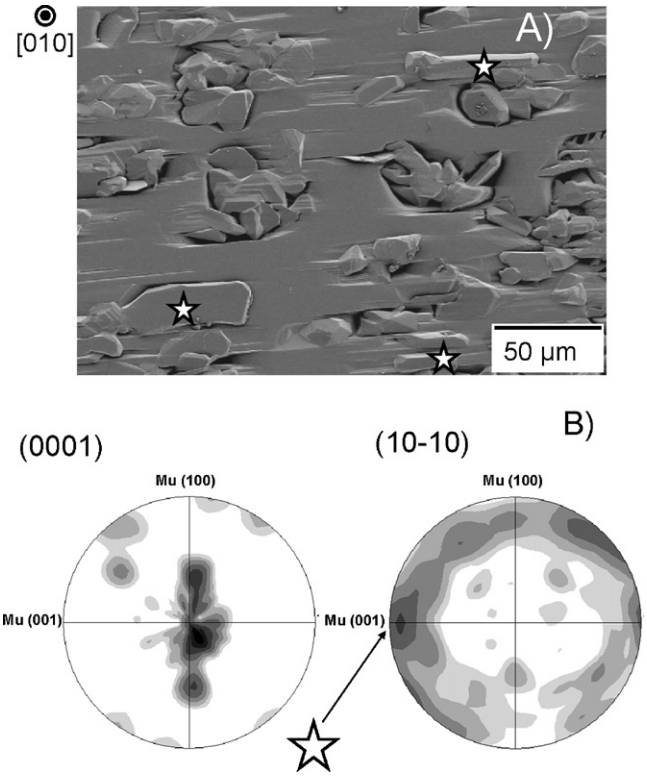

Fig. 2. Alumina formation on water vapor-treated (1200 °C, 3 h) mullite single crystal sections cut parallel to (0 1 0). (A): Microstructure; (B) pole figures of basal (0 0 0 1) and prismatic (1 0 –1 0) planes of α-Al_2O_3. α-Alumina crystals are predominantly oriented according to [0 0 0 1]Cor || [0 1 0]Mul. Prismatic crystal planes of most α-alumina crystals display random distribution, but elongated α-alumina crystals typically have the in-plane orientation relationship $(1\,0\,-1\,0)_{\alpha\text{-}Al_2O_3} \| (0\,0\,1)_{Mullite}$ (star symbol).

do occur. The orientation of the elongated alumina crystals is almost uniform with the longitudinal axis being oriented parallel to the *c*-axis of the starting mullite single crystal. The amount of newly formed alumina on $(0\,0\,1)_{Mullite}$ and $(0\,1\,0)_{Mullite}$ is virtually the same, though corrosive pitting is more pronounced on $(0\,1\,0)_{Mullite}$.

Information on the orientation relationships between parent mullite single crystals and the newly formed α-alumina as evidenced by EBSD are shown in Figs. 1B and 2B. α-Alumina crystals grown on $(0\,0\,1)_{Mullite}$ are found to be predominantly oriented according to $[0\,0\,0\,1]_{\alpha\text{-}Al_2O_3} \| [0\,0\,1]_{Mullite}$, with a deviation of up to 20°. The prismatic α-alumina crystal planes $\{0\,1\,-1\,0\}$ display a virtually random distribution around this $[0\,0\,0\,1]_{\alpha\text{-}Al_2O_3} \| [0\,0\,1]_{Mullite}$ axis (Fig. 1B). Thus, in a first approximation, the orientation relationship between α-alumina crystals and mullite can be described as fiber texture.

α-Alumina crystals grown on $(0\,1\,0)_{Mullite}$ display the orientation relationship $[0\,0\,0\,1]_{\alpha\text{-}Al_2O3} \| [0\,1\,0]_{Mullite}$. This means that again the *c*-axis of the newly formed α-alumina crystals is parallel to the normal of the parent mullite crystal face. However, there is no strict fiber texture, but certain preferential in-plane orientations do appear: typically, the large, elongated α-alumina crystals show the in-plane orientation relationship $(1\,0\,-1\,0)_{\alpha\text{-}Al_2O_3} \| (0\,0\,1)_{Mullite}$ (Fig. 2B, star symbol).

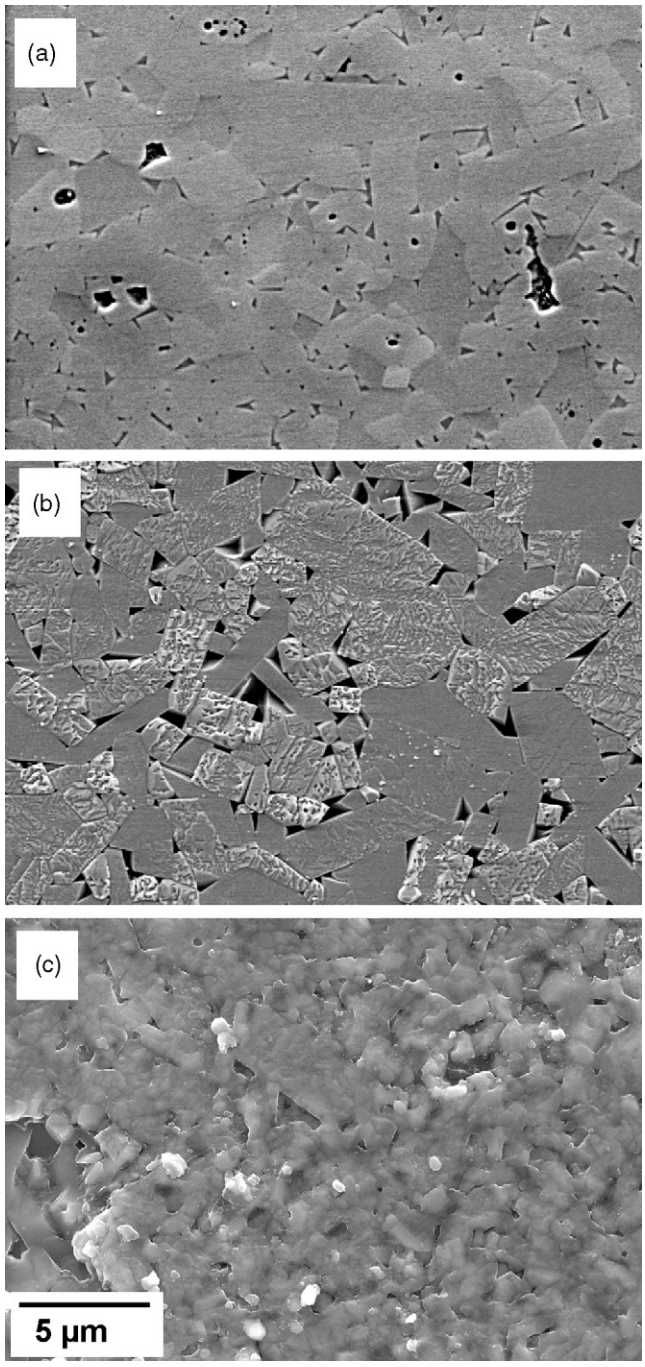

Fig. 3. Mullite ceramics before (a) and after water vapor-treatment (1200 °C) for 1.5 h (b) and 3 h (c). Note the selective corrosive attack after 1.5 h vapor treatment. After 3 h a continuous layer of alumina has been formed on top of the mullite surface.

3.2. H_2O vapor-treated polycrystalline mullite ceramics

The microstructure of mullite ceramics before and after vapor-treatment for 1.5 and 3 h, respectively, is shown in Fig. 3(a–c). The 1.5 h treatment results in a selective corrosive attack: a certain fraction of grains is significantly corroded with superficial α-alumina formation, whereas other grains are virtually unaffected (Fig. 3b). EBSD investigations on mullite grains showing strong or little corrosive attack, respectively, provide

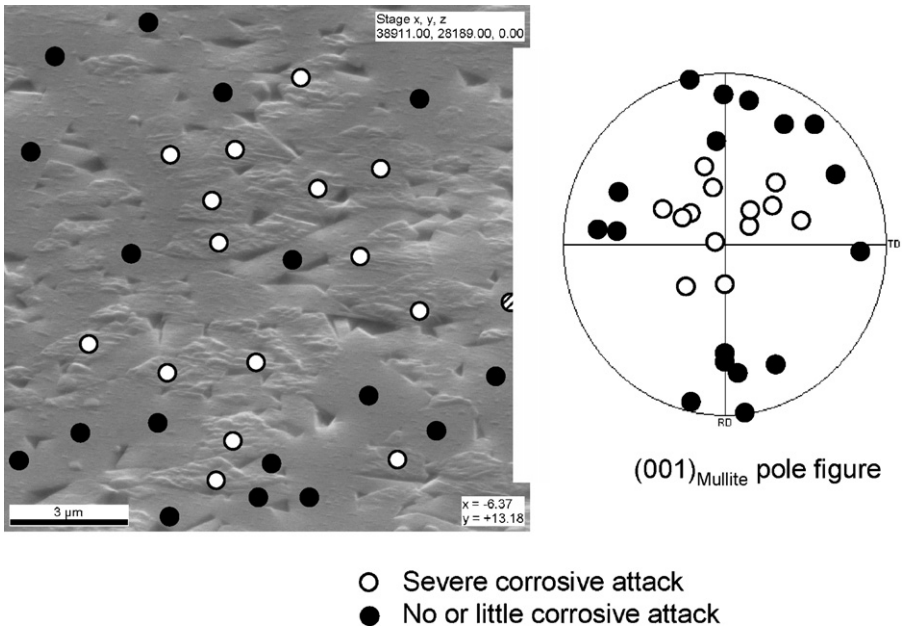

Fig. 4. Non-isotropy of selective mullite corrosion: EBSD analyses reveal that preferential corrosion occurs if mullite grain surfaces are more or less parallel to crystallographic (0 0 1) planes.

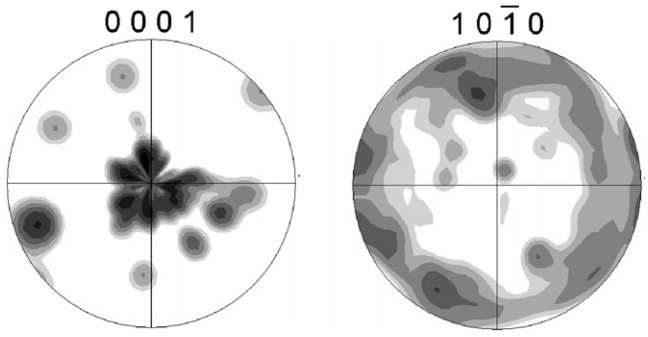

Fig. 5. Pole figures of basal (0 0 0 1) and prismatic (1 0 $\bar{1}$ 0) planes of α-Al_2O_3 (corundum) on a polycrystalline mullite ceramics (1200 °C, 3 h water vapor treatment). Basal planes of α-alumina crystals are predominantly oriented parallel to the mullite surface, whereas prismatic corundum crystal planes display random distribution.

information on the non-isotropy of the transformation reaction (Fig. 4): obviously, grain surfaces oriented parallel or nearly parallel to the crystallographic (0 0 1) planes undergo the mullite/alumina conversion, whereas grain surfaces of (*h k* 0) type remain almost unchanged after 1.5 h water vapor treatment at 1200 °C. H_2O water vapor treatment of 3 h leads to the formation of a complete thin surface layer of alumina (Fig. 3c). Fig. 5 indicates the orientation of the newly formed α-alumina crystals: again, the Al_2O_3 crystals exhibit a fiber texture with the *c*-axis oriented parallel to the surface normal of the ceramic body.

4. Discussion

4.1. Comparison between mullite single crystals and polycrystalline mullite ceramics

Experimental data suggest that the early stages of water vapor-induced mullite-alumina conversion of single crystal and polycrystalline materials are controlled by different mechanisms. Corrosion experiments performed on single crystal mullite platelets oriented parallel to (0 0 1) and (0 1 0) do not provide evidence for non-isotropic kinectics of alumina formation, since the amount of newly formed alumina is virtually the same for both orientations. In contrast, EBSD investigations of polycrystalline samples unambiguously prove higher corrosion rates parallel to the crystallographic *c*-axis whereas other directions seem to be unaffected after our short-term vapor treatments. Moreover, single crystal mullite and polycrystalline ceramics show a strong difference in the nucleation density of newly formed alumina. Alumina crystal density is high in case of polycrystalline samples (ca. 5×10^6 /mm^2, as estimated from Fig. 3c) but low if mullite single crystals were employed (ca. 5×10^3 /mm^2 (see Figs. 1A and 2A).

As a matter of fact mullite crystals of polycrystalline ceramics and melt-grown mullite single crystals do not only differ in microstructure but also display deviating compositions. Mullite crystals of sintered ceramics typically have the stoichiometric composition 60 mol% (72 wt.%) Al_2O_3, 40 mol% (28 wt.%) SiO_2, while in melt-derived single crystals the peritectic composition higher in Al_2O_3 is frozen in (Table 1, Fig. 6). Thus, unlike mullite crystals in ceramics, mullite single crystals are supersaturated in Al_2O_3. Therefore, in single crystals, there is a priori a driving force for alumina precipitation. In dry and clean environments, the alumina supersaturation of melt-grown mullite crystals typically is retained, but hot water vapor assumingly facilitates the alumina precipitation process by hydroxylation of mullite[4] ("Hydrolytic weakening"). A different situation exists for the stoichiometric mullite crystals of the ceramic sample: there is no initial supersaturation being a driving force for alumina precipitation. In that case only due to significant $Si(OH)_4$ volatilization, i.e. a corrosion in the strict sense, the composition of the mullite crystals gradually shift towards Al_2O_3, thus

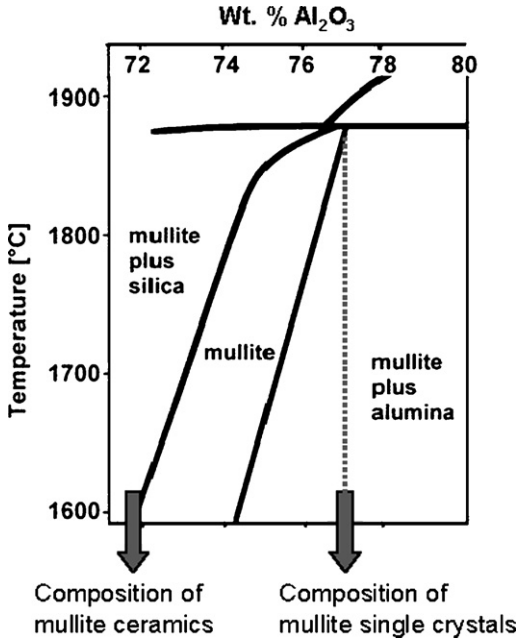

Fig. 6. Mullite region of the SiO_2–Al_2O_3 phase diagram (after Ref.[13]).

leading to the formation of α-alumina if a certain supersaturation is reached. Unlike the precipitation process in mullite single crystals, corrosion of mullite obviously is a non-isotropic process. The EBSD-analysis revealed that the corrosive attack preferentially proceeds along the crystallographic *c*-axis. Perpendicular to the structural chains the corrosive attack via $Si(OH)_4$ volatilization is significantly lower.

Vapor corrosion of mullite reflects the non-isotropy of chemical bonding and can be rationalized in terms of Hartmann and Perdok's PBC theory.[10] The periodic bond chains (PBC) of a crystal are crystallographic directions in which atoms are connected to each other by strong energetic bonds. Crystal growth preferentially occurs in PBC direction. Crystal planes which are perpendicular to predominant PBC directions have high specific surface energy and hence these planes are susceptible to dissolution. In case of mullite, it can be assumed that the predominant PBC vector is determined by the structural chains of AlO_6 octahedra and $(Si,Al)O_4$-tetrahedra running parallel to the crystallographic *c*-axis. Correspondingly, the typical growth direction of mullite is [0 0 1]. The [0 0 1] PBC vector gives rise to high surface energy of (0 0 1) planes which was recently verified experimentally by Braue et al. on the basis of wetting studies.[11] Thus, it can be assumed that preferential corrosive attack of mullite surfaces being oriented more or less perpendicular to the crystallographic *c*-axis (see Fig. 4) is due to the high specific surface energy of (0 0 1) planes.

4.2. Orientation of newly formed α-Al_2O_3

Iwai et al. investigating the decomposition of mullite in a propane-oxygen flame observed the following orientation relationship between newly formed α-alumina and mullite $(3\,1\,0)_{Mullite} \| (0\,0\,0\,1)_{\alpha\text{-}Al_2O_3}$; $[0\,0\,1]_{Mullite} \| [1\,-1\,0\,0]_{\alpha\text{-}Al_2O_3}$. This orientation relationship was interpreted in terms of approximately close packing of oxygen atoms in the $(3\,1\,0)_{Mullite}$ planes which was may coincide with the close-packed oxygen arrangement in the basal plane (0 0 0 1) of α-alumina. In the present study, the above mentioned orientation relationship was not observed. Actually, a strict orientation relationship between parent mullite and newly formed α-alumina cannot be expected under the present conditions, as our investigations have shown that the *c*-axis of newly formed α-alumina crystals are in general parallel to the macroscopic mullite surface normal (see Figs. 1B and 2B 4). This finding is interpreted as a general nucleation phenomenon of α-Al_2O_3 rationalized in terms of minimizing the transformation-induced elastic strain energy: it can be assumed that the elastic strain of disc-shaped α-Al_2O_3 newly formed on a mullite surface is reduced if the direction of its highest Young's modulus sticks out of the sample surface. Actually, the out-of-plane [0 0 0 1]-direction of α-Al_2O_3 corresponds to the direction of its highest Young's modulus[12] The preferential orientation relationship between mullite and the elongated alumina crystals occurring on the (0 1 0) single crystal surface is discussed in detail in Ref. 8.

Acknowledgements

The authors thank Dr. B. Hildmann and Mr. K. Baumann (DLR) for the preparation of oriented mullite sections. Mrs. K. Angenendt (MPIE) assisted in EBSD data collection which is gratefully appreciated.

References

1. Schneider, H. and Komarneni, S., ed., *Mullite*. Wiley VCH, Weinheim, 2005.
2. Ueno, S., Jayaseelan, D. D., Kondo, N., Ohji, T. and Kanzaki, S., Water vapor corrosion of mullite containing small amount of sodium. *Ceram. Int.*, 2005, **31**, 177–180.
3. Fritsch, M., Klemm, H., Herrmann, M. and Schenk, B., Corrosion of selected ceramic materials in hot gas environment. *J. Eur. Ceram. Soc.*, 2006, **26**, 3557–3565.
4. Rüscher, C., Shimada, S. and Schneider, H., High temperature hydroxylation of mullite. *J. Am. Ceram. Soc.*, 2002, **85**, 1616–1618.
5. Iwai, S., Watanabe, T., Minato, I., Okada, K. and Morikawa, H., Decomposition of mullite by silica volatilization. *J. Am. Ceram. Soc.*, 1980, **63**, 44–46.
6. B. Hildmann, W. Braue, to be published.
7. Eils, N., Rüscher, C., Shimada, S., Schmücker, M. and Schneider, H., High-temperature hydoxylation and surface corrosion of 2/1 mullite single crystals in water vapor environments. *J. Am. Ceram. Soc.*, 2006, **89**, 2887–2894.
8. Schmücker, M., Mechnich, P., Zaefferer, St. and Schneider, H., The high temperature mullite/ α-alumina conversion in rapidly flowing water vapor. *Scripta Mater.*, 2006, **55**, 1131–1134.
9. Saalfeld, H. and Guse, W., Mullite single crystal growth and characterization. *Ceram. Trans.*, 1990, **6**, 73–101.
10. Hartman, P. and Perdok, W. G., On the relations between stucture and morphology of crystals. *Acta Crystallogr.*, 1955, **8**, 525–529.
11. Braue, W., Hildmann, B., Schneider, H., Eldred, B. T., Ownby, P. and Darell, P., Reactive wetting of mullite $Al_2[Al_{2+2x}Si_{2-2x}]O_{10-x}$ by yttrium-aluminosilicate and borosilicate glasses. *J. Mater. Sci.*, 2005, **40**, 2335–2340.
12. Dörre, E. and Hübner, H., *Alumina*. Springer-Verlag, Berlin, 1984, p. 75.
13. Klug, F. J., Prochazka, S. and Doremus, R. H., Alumina-silica phase diagram in the mullite region. *J. Am. Ceram. Soc.*, 1987, **70**, 750–759.